

**Incomplete relaxation in a two-mass one-dimensional self-gravitating system**

Kenneth R. Yawn and Bruce N. Miller

*Department of Physics, Texas Christian University, Fort Worth, Texas 76129, USA*

(Received 1 July 2003; published 24 November 2003)

Due to the apparent ease with which they can be numerically simulated, one-dimensional gravitational systems were first introduced by astronomers to explore different modes of gravitational evolution. These include violent relaxation and the approach to thermal equilibrium. Careful work by dynamicists and statistical physicists has shown that several claims made by astronomers regarding these models were incorrect. Unusual features of the evolution include the development of long lasting structures on large scales, which can be thought of as one-dimensional analogs of Jupiter's red spot or a galactic spiral density wave or bar. The existence of these structures demonstrates that in gravitational systems evolution is not entirely dominated by the second law of thermodynamics and also appears to contradict the Arnold diffusion ansatz. Thus it is correct to assert that the one-dimensional planar sheet gravitational system is the nonextensive analog of the Fermi-Pasta-Ulam model of dynamical systems. This paper is an extension of a preliminary study where we conclusively showed mass segregation and equipartition of kinetic energy in a two-mass planar sheet system for the first time. Here we employ both mean-field theory and dynamical simulation to more thoroughly probe the statistical and ergodic properties of these systems. Valuable information is obtained from local and global time averaging, and temporal and spatial correlation functions. Using these tools we show that the system appears to approach the equilibrium distribution on very long time scales, but the relaxation is incomplete.

DOI: 10.1103/PhysRevE.68.056120

PACS number(s): 05.90.+m, 05.70.-a, 05.20.-y, 95.10.Fh

**I. INTRODUCTION**

The study of one-dimensional models has historically been motivated by the simplicity of the physical systems. Many of these systems have analytical or nearly analytical solutions. In other cases, although the system is physically simple, the equations do not admit an analytical solution but are nevertheless straightforward to set up and dynamically simulate on a computer. One-dimensional systems were among the first simulations done on computing machines in the late 1940s and early 1950s. One of the first and most famous numerical experiments was conducted by Fermi, Pasta, and Ulam in 1955 on a one-dimensional array of coupled oscillators with force terms that were small perturbations from linearity [1]. The unexpected nonergodic results of the experiment would cause an explosion in dynamical physics and chaos theory several years later. One-dimensional models of gases have been studied extensively in statistical mechanics and one-dimensional lattice models have been used in solid state physics to study metal alloys, magnetic spin systems, glasses, phonon propagation, electronic bands, and a host of other systems. Due to the added complexity of the physics in higher dimensions, one-dimensional systems are often used as simpler models of actual three-dimensional systems.

A central problem for stellar dynamics is the determination of the time scale for the relaxation of an isolated, gravitationally bound system, such as a galaxy or a globular cluster. A primary reason for the difficulty is the extremely complicated nature of physics in three dimensions. Since the 1960s, the one-dimensional (1D) self-gravitating system has been used as the simplest model for studying the dynamical properties of gravitational systems, such as relaxation and diffusion. The study of 1D gravitational systems is motivated by two primary factors. The first is the hope that some of the

general features of the 1D system may translate to 3D astrophysical systems, perhaps giving some unique insight into the underlying physics. The second is that 1D systems appear on the surface to be relatively simple but often exhibit interesting and unexpectedly complex behavior. This has certainly proved true over the many years that these systems have been studied.

Correlating results derived from one-dimensional gravitational systems to three dimensions is a difficult task, since it is well known that dimensionality plays a critical role in many physical phenomena. Despite this difficulty, several important similarities do exist between one- and three-dimensional gravitational systems and these are summarized below.

(1) Both 1D and 3D systems have long range unscreened gravitational forces.

(2) For systems containing a large number of particles existing in a stationary state, the distribution of particle positions and velocities is governed approximately by the Vlasov equation for incompressible fluid flow [Eq. (1)].

(3) Evolution of the systems from a highly nonstationary state appears to go through a period of violent relaxation after which the distribution quickly settles down to a quasi-equilibrium state.

It is worth noting that three-dimensional gravitational systems suffer from several problems that do not exist in one dimension.

(1) Through three body or higher-order interactions, particles can gain enough energy to escape (or evaporate) from the system.

(2) Through three body or higher-order interactions, particles can lose enough energy to form gravitationally bound pairs (binaries).

(3) A singularity exists in the gravitational force at  $r = 0$ .

To manage these problems in practical computer simulations, two- and three-dimensional programs require elaborate cutoff schemes for the gravitational potential. In contrast, since the gravitational field in one dimension is uniform, the phase space is compact, and the equations of motion are parabolic and easily solvable on a computer without the use of slow integration techniques. This allows the completion of very long simulations of systems with moderately large  $N$  in a few days or weeks on desktop workstations.

Large astrophysical systems, such as galaxies, may contain upwards of  $10^{11}$  stars. Gravitational systems are unlike gaseous systems (driven by true short-range interactions) or plasmas (where the range of the electric force is limited by Debye screening) in that each particle continuously feels the effect of all the others. As the number of particles in the system is increased, however, the effect of any single particle relative to the background composed of all other particles decreases as  $1/N$ . In the limit that  $N \rightarrow \infty$ , while the total mass is kept constant, only the long-range interaction of the particle with the continuous background field remains. In this “mean-field” approximation, the evolution of large gravitational systems is exactly described by the Vlasov, or collisionless Boltzmann equation, Eq. (1) [2],

$$\frac{\partial f}{\partial t} + \mathbf{v} \cdot \frac{\partial f}{\partial \mathbf{x}} - \nabla \Phi \cdot \frac{\partial f}{\partial \mathbf{v}} = 0, \quad (1)$$

where  $\Phi$  is a solution of the Poisson equation. For systems with finite  $N$ , the solution to Eq. (1) provides a short-time approximation to the single-particle distribution function. In one dimension, the Vlasov equation describes the flow of an incompressible fluid in  $\mu = (x, v)$  space, where the  $\mu$  space is a projection into the  $(x, v)$  plane of a point in the  $2N$ -dimensional phase space. The  $\mu$  space then contains  $N$  points, each of which represents the position and velocity of a particle in the system. In the limit that the number of particles,  $N$ , approaches infinity while constraining the total system energy and mass to constants, the system can be described as a continuous fluid in  $\mu$  space. This limit is often referred to as the Vlasov limit. Liouville’s theorem states that the area of an element in the  $\mu$  space is constant under the action of the Hamiltonian. Therefore, the flow of this fluid in  $\mu$  space is incompressible and obeys the Vlasov equation.

Following a suggestion by Oort [3], the one-dimensional self-gravitating system (OGS) was first considered as a model for the motion of stars perpendicular to the plane of a highly flattened galaxy by Camm [4]. Camm’s analysis was the first to apply the Vlasov equation to the 1D system, by assuming that the long-range gravitational forces wash out any effects of stellar encounters, making the system essentially collisionless. With the assumption of separability of the distribution function, Camm derived the stationary isothermal solution to the Vlasov equation. In 1967, Lynden-Bell [5] published a theory describing a rapid relaxation process termed “violent relaxation,” in which large changes in the gravitational potential are driven by rapid fluctuations in the mass distribution. Cohen and Lecar [6] used the 1D system to study Lynden-Bell’s theory of violent relaxation and found that the systems do relax to a stationary state after a short

time, but not necessarily to those predicted by Lynden-Bell’s theory. Later, Cuperman, Hartman, and Lecar [7] investigated violent relaxation and the applicability of Vlasov dynamics. A breakthrough came when Rybicki [8] first derived the exact single-particle equilibrium distribution function for the discrete one-dimensional self-gravitating system in both the canonical and the microcanonical ensemble for arbitrary  $N$ . In the Vlasov limit, these distributions were shown to converge to the isothermal solution of the Vlasov equation found earlier by Camm.

In principle, additional information can be obtained from the statistical distribution of particle pairs. Monaghan [9], and Fukui and Morita [10] showed that for the OGS in the Vlasov limit, the two-particle distribution function is the product of the single-particle distribution functions, and corrections are of order of  $N^{-1}$ . In contrast with the single-particle distribution, at the present time an analytical expression for the pair distribution is not known, and therefore there is no exact method for computing the effects of two-particle or higher-order correlations in a system with a finite population.

Computer simulations of finite population 1D systems show that they tend to progress through several quasiequilibrium (approximately stationary) states as they evolve from arbitrary initial conditions. These quasiequilibrium states often last for extremely long times. When a simulation is initiated from a nonstationary distribution, fluctuations caused by the changes in the mean-field potential rapidly decay resulting in a state of microscopic relaxation. This process is frequently referred to as violent relaxation [5]. In this state, the system is virialized (i.e.,  $2\langle KE \rangle / \langle PE \rangle \approx 1$ ), and the system energy is distributed approximately equally between all the particles in what is called equipartition of total energy. The time scale for microscopic relaxation is distinguished from the much longer time scale for macroscopic relaxation to thermal equilibrium.

For an  $N$ -particle 1D gravitational system, a single point in the  $2N$ -dimensional phase space ( $\Gamma$  space) defines the state of the system. The system trajectory in this space is governed by Hamiltonian dynamics as the state of the system changes. Because of inexact knowledge of initial conditions, a probability density can be defined that indicates a range of possible states that the system can occupy. For a conservative system, such as the OGS, the total energy is a constant and defines an isolating integral that will restrict the trajectory of the system to the energy hypersurface  $S_E$  defined by the Hamiltonian.

In order for a system to approach equilibrium from an arbitrary initial condition, it must exhibit the properties of both ergodicity and mixing [11]. A system is ergodic if the phase-space average of a dynamical quantity is equal to the time average. Ergodic flow can exist only if there are no other isolating integrals that will prevent the system from sampling the entire energy surface. Ergodicity implies that all areas of the energy surface are equally accessible and that all states on the energy surface are equally probable, thus the system will spend equal time in equal areas of the phase space. Qualitatively, mixing is described as the spreading out of the phase-space probability density as the system evolves.

If a system is initially far from equilibrium, then the probability density may fill a localized area on the energy surface. As the system evolves under the action of the Hamiltonian, this area will move over the energy surface. If the system is mixing, the probability density will begin to spread itself out, eventually covering the entire energy surface equally while preserving its initial area.

When investigating gravitating systems it is important to keep several things in mind. Often, computer simulations of gravitating systems (which are necessarily finite in the population) are studied with, and compared to, Vlasov dynamics. The Vlasov limit is a singular limit in the sense that infinite time averages of dynamical quantities cannot yield the expected equilibrium results if the limit  $N \rightarrow \infty$  is taken prior to the  $T \rightarrow \infty$  limit. This follows from the fact that a true Vlasov system has an infinite number of stable stationary solutions and Casimir invariants, and therefore does not converge to the unique maximum entropy state; i.e. Vlasov dynamics does not obey the second law of thermodynamics. This has been demonstrated by numerical integration of the Vlasov equation for the OGS where it was shown that structures in the  $\mu$  space appear to persist indefinitely without any sign of dissipation [12]. On the other hand, a finite population system may sample an approximately stationary state that closely resembles a stationary Vlasov solution for a long time. However, for the system with finite population, it is not truly stationary and will slowly drift away due to discrete particle effects. Therefore an infinite time limit  $T \rightarrow \infty$  of a dynamical quantity in the discrete system followed by the Vlasov limit  $N \rightarrow \infty$  will give the equilibrium solution provided the system is mixing.

Prior to 1982 the prevailing thought was that the OGS should relax to equilibrium from an arbitrary initial state in a time scale on the order of  $N^2 t_c$ , where  $t_c$  is the approximate time it takes a particle to make one complete crossing (full oscillation) in the system [13]. However, Wright, Miller, and Stein [14] showed that there was no relaxation in a time of  $2N^2 t_c$ . Subsequent studies by Leuwel, Severn, and Rousseeuw [15] showed relaxation in a time  $N t_c$  from special initial states chosen close to equilibrium. From that work they predicted relaxation on this same scale for any initial system chosen close to equilibrium. Reidl and Miller [16] refuted that claim by showing that the relaxation time depends very sensitively on the initial quasiequilibrium state chosen. Comparison of the position distribution of computer simulations with the prediction of Rybicki's discrete  $N$ -particle distribution function continued to show major discrepancies even after long run times. Particles were more concentrated toward the center and toward the outer edges than predicted. In addition, Reidl and Miller [17,18] did ergodic studies of 1D systems containing from 2 to 20 particles looking for evidence for strong ergodic behavior which would result in eventual thermal equilibrium. They found a transition at  $N=11$  particles where previously stable regions of the phase space became ergodic and mixing. In their subsequent study of early relaxation, Reidl and Miller [19] showed a maximum mixing in phase space when the system population was on the order of  $N=30$ .

During this same time period, Tsuchiya *et al.* [20,21] began studying the approach to equilibrium of the single-mass OGS using a measure of the equipartition of total system energy among all the particles. This measure  $\Delta(t)$  is the deviation of the average energy per particle from the theoretical equipartition value given by the virial theorem. These studies showed that after an initial short period of microscopic relaxation in which  $\Delta(t)$  is approximately constant,  $\Delta(t)$  steadily declines in a linear fashion on a log-log scale indicating a power-law decay. After some period of time a large peak appears which was interpreted as the onset of thermal equilibrium. Shortly afterward however, using both small and large- $N$  systems [22] (Paper I), we demonstrated that this phenomena was not the onset of equilibrium but that it might be evidence for the system becoming trapped for long periods of time in restricted regions of the phase space. Typically, if the system is followed long enough, many peaks are seen to appear after the first initial large peak, indicating periods where the system is restricted from equally exploring the entire energy hypersurface. Following up on their earlier work with a study of the distribution of particle energies, Tsuchiya *et al.* [23] showed evidence for continual transitions back and forth between a state closely mimicking the isothermal distribution (isothermal-like) to a far from equilibrium distribution (transient or itinerant state). This will be referred to as the transitional distribution period.

It was recognized by a number of investigators that an alternative approach for studying convergence to equilibrium could be found by employing two different mass species in the OGS [24,25]. The eventual occurrence of equilibrium would then be characterized by the equipartition of the kinetic energy as well as the spatial segregation of the heavy and light particles. However, perhaps due to algorithm and hardware limitations, early attempts failed to obtain a convincing result. To complement Tsuchiya's investigations of the single-component system, we investigated the evolution of a two-component system consisting of equal populations of each species with a 3:1 mass ratio [26] (Paper II). We observed that both equipartition of kinetic energy and mass segregation occurred after approximately  $10^6$  system crossing times. To our knowledge, this was the first time that this phenomenon was conclusively demonstrated for this system. The time scale is on the same order as the occurrence of the transitional distribution period discussed above for a single-component system.

In other recent work dynamicists have studied the average divergence of phase-space trajectories of the OGS. Positive Lyapunov exponents are attributes of strong ergodic properties, such as mixing. Earlier, Tsuchiya *et al.* [20] and more recently Milanovic *et al.* [27] and Tsuchiya and Gouda [28] investigated the Lyapunov spectra of the OGS. At this time there are unresolved questions concerning the convergence of the spectra to a universal scaling function as  $N$  becomes large. Power-law dependence on population was found for both maximum and minimum exponents, both of which decrease with increasing  $N$ . This suggests an approach to a more integrable system as the population increases. Other recent work has attempted to relate this model more directly to physical stellar systems such as globular clusters [29].



While the preceding review has focused on studies of an isolated one-dimensional gravitational system, it should be noted that they have also played a useful role in studies of structure formation in cosmology. By including the Hubble expansion in the dynamical evolution it is possible to demonstrate the formation of clusters and “voids” in the  $\mu$  space [30,31]. A few models have been considered and, in common with galaxy observations, they demonstrate a bifractal distribution of matter. They also provide the only model that exactly follows the Zeldovich ansatz [32,33] between crossings [34].

This paper continues the investigation of multiple-mass component systems started previously by us in Paper II. There, as a preliminary study, a single system size and mass ratio was investigated. The results conclusively showed for the first time mass segregation and equipartition of kinetic energy. Here the complete mean-field theory is developed for an equilibrated two-mass system in the Vlasov limit using the maximum entropy principle. Coupled differential equations for the resulting density functions in the  $\mu$  space for each mass species are derived and can be integrated numerically for any given temperature and mass ratio. They are used to estimate the particle distribution of systems with finite population in equilibrium.

Dynamical simulations of systems with varying population ( $N=16, 32, 64, 128$ ) and three different mass ratios (2:1, 3:1, and 5:1) were carried out on the computer. The observed equipartition of kinetic energy (the ratio of the kinetic energies of the heavy to light masses) and mass segregation were compared with the theoretical predictions. In addition, an extensive range of statistical measures calculated from the numerical simulations are used to investigate properties that cannot be predicted from mean-field theory. These include the spatial correlation between particle positions, the time correlation of kinetic energy fluctuations, and a measure of the rate of relaxation toward equilibrium. As shown below, surprising results are obtained, some of which appear to contradict the conventional wisdom concerning gravitational systems.

## II. DESCRIPTION OF THE SYSTEM

The two-mass component 1D self-gravitating system is a collection of  $N$  labeled, planar sheets, each of constant mass density, infinite in the  $y$ - $z$  plane, which are constrained to move along the  $x$  axis under their mutual gravitational attraction. It is convenient to introduce an auxiliary labeling which increases in the direction of increasing  $x$ . Therefore, in specifying the auxiliary particle number, say  $j$ , the acceleration of that particle is uniquely defined and vice versa.

Only gravitational forces are considered (i.e., no short-range interactions). Therefore, on crossing, they merely pass through one another. Since the sheets are infinite in extent, the gravitational field in the  $x$  direction is uniform. Clearly, the system can be thought of as a collection of particles each with mass  $m_j$  constrained to move in one dimension. The gravitational acceleration is found through Poisson's equation

$$-\frac{\partial A(x,t)}{\partial x} = 4\pi G\rho(x,t), \quad (2)$$

where  $\rho(x,t)$ , the mass density, is given by

$$\rho(x,t) = \sum_{j=1}^N m_j \delta(x-x_j(t)) \quad (3)$$

and  $G$  is the universal gravitational constant and  $\delta$  is the Dirac delta function. Therefore,

$$A(x,t) = 2\pi G \sum_{j=1}^N m_j S(x-x_j(t)), \quad (4)$$

where  $S(x)$  is defined as

$$\begin{aligned} -1, & \quad x > 0 \\ S(x) = 0, & \quad x = 0 \\ 1, & \quad x < 0. \end{aligned} \quad (5)$$

The acceleration experienced by the  $j$ th particle from the left therefore depends only on the difference in the mass of particles on the right and on the left and can be expressed simply as

$$A_j = 2\pi G(M_R - M_L). \quad (6)$$

At the instant when two particles cross, the velocities do not change. Therefore the velocity of each particle varies *continuously* in time while, at a crossing, each particle experiences a discrete jump in the acceleration. Between crossings the particle positions evolve quadratically in time. The change in the acceleration of the  $j$ th particle during a crossing is

$$\Delta A_j = \pm 4\pi G m_{j\mp 1} \quad (7)$$

where the top signs correspond to the case where the  $j$ th particle has a crossing with a particle coming from the left and the bottom signs to a crossing from the right. The Hamiltonian of the system is

$$H = \sum_{j=1}^N \frac{p_j^2}{2m_j} + 2\pi G \sum_{j<i} m_i m_j |x_i - x_j|, \quad (8)$$

where  $p_j$ ,  $x_j$ , and  $m_j$  are the momentum, position, and mass of the  $j$ th particle, respectively. It is customary to define the characteristic period of a particle in the system as  $t_c = (G\rho_0/\pi)^{-1/2}$ , where  $\rho_0$  is the equilibrium mass density evaluated at the origin and  $G$  is the universal gravitational constant. This represents a typical period of oscillation of a particle in the system.

Since the potential energy is a linear homogeneous function of the coordinates, all dependence on parameters can be scaled away by introducing convenient units as follows:

$$L = \frac{2E}{3\pi GM^2}, \quad V = \left[ \frac{4E}{3M} \right]^{1/2}, \quad T = \left[ \frac{1}{\pi MG} \right] \left[ \frac{E}{3M} \right]^{1/2}, \quad (9)$$

where  $L$  is the length,  $V$  is the velocity,  $T$  is the time,  $G$  is the universal gravitational constant, and  $E$  and  $M$  are the total system energy and mass, respectively. The dimensionless units of acceleration, velocity, position, and time are then given by

$$A \rightarrow a = \frac{A}{2\pi MG}, \quad V \rightarrow v = \frac{V}{2} \left[ \frac{3M}{E} \right]^{1/2},$$

$$X \rightarrow x = \left[ \frac{3\pi M^2 G}{2E} \right] X, \quad T \rightarrow \tau = \frac{t}{T}. \quad (10)$$

For simplicity set

$$M = 1 \quad \text{and} \quad 2\pi G = 1, \quad (11)$$

making the total energy of the system  $E = \frac{3}{4}$ , and the characteristic period of oscillation  $t_c = 2\pi\tau$ . These units will be adopted throughout the remainder of this paper.

### III. VLASOV (MEAN-FIELD) THEORY FOR THE TWO-MASS SYSTEM

Here we derive the equilibrium solution for the probability distribution and mass density of the two-mass system in the Vlasov (or mean-field) limit. In this limit all correlations between particles vanish and, therefore, the derivation begins with the assumption of statistical independence. Coupling with this assumption, Eq. (12), with the Hamiltonian Eq. (8) an expression, Eq. (19), is obtained for the entropy. Subject to constraints on the energy and normalization of probability, the entropy is maximized using the method of Lagrange multipliers, Eqs. (21) and (22). The solution yields the reduced partition functions, Eqs. (36), and the form of the particle density functions, Eq. (37). With these and the boundary conditions at the origin and at infinity, Poisson's equation gives a first-order differential equation for the potential  $\varphi$  in the two-mass mean-field theory, Eq. (49). The remaining constants  $A$  and  $B$  are solved with the help of Eq. (53). A final integral for  $x$  as a function of  $\varphi$  is obtained and solved numerically. Inversion of the solution yields  $\varphi$  as a function of  $x$ . All of these elements can be applied to Eq. (37) to calculate the density of each species as a function of position that can be compared with results obtained from simulations.

Consider the  $N$ -particle distribution function  $f^{(N)}(x_i, v_i)$  for a system with two mass types. In the Vlasov limit

$$f^{(N)} = \prod_a f_a \prod_b f_b \quad (12)$$

is the product over the single-particle distribution functions of each mass type, where

$$\prod_a f_a = \prod_j f_a(x_j, v_j), \quad \text{etc.} \quad (13)$$

The two distribution functions,  $f_a$  and  $f_b$ , will independently satisfy the Vlasov or Collisionless Boltzmann equation,

$$\frac{\partial f_a(x, v)}{\partial t} + v(t) \frac{\partial f_a(x, v)}{\partial x} - \frac{\partial \varphi(x)}{\partial x} \frac{\partial f_a(x, v)}{\partial v} = 0, \quad (14)$$

$$\frac{\partial f_b(x, v)}{\partial t} + v(t) \frac{\partial f_b(x, v)}{\partial x} - \frac{\partial \varphi(x)}{\partial x} \frac{\partial f_b(x, v)}{\partial v} = 0, \quad (15)$$

where the acceleration

$$a = \frac{\partial v}{\partial t} = -\nabla \varphi(x). \quad (16)$$

For a stationary distribution, the functions are independent of time so the first terms on the left are expressly zero. The entropy of the system is given by

$$S = -k \text{Tr}[P \ln P]$$

$$= -k \int d\Gamma f^{(N)} \ln f^{(N)}, \quad (17)$$

where  $P$  is the probability that the system is at a particular point in the phase space and  $k$  is Boltzmann's constant. Therefore, from Eq. (12),

$$S = -k \left[ \int d\Gamma_a \prod_a f_a \ln \prod_a f_a + \int d\Gamma_b \prod_b f_b \ln \prod_b f_b \right] \quad (18)$$

which reduces to

$$S = -k \left[ N_a \int d\mu_a f_a \ln f_a + N_b \int d\mu_b f_b \ln f_b \right]. \quad (19)$$

Let  $\alpha_a = N_a/N$  and  $\alpha_b = N_b/N$  where  $N_a$  and  $N_b$  are the numbers of particles of mass types  $a$  and  $b$  respectively, i.e.,  $\alpha_a$  and  $\alpha_b$  are the fractions of the total number of particles of each type. Then the total entropy per particle is

$$s \equiv \frac{S}{kN} = -\alpha_a \int d\mu_a f_a \ln f_a - \alpha_b \int d\mu_b f_b \ln f_b. \quad (20)$$

Expressed in this form,  $s$  survives the Vlasov limit. Next we construct the extremum of  $s$  given the constraints

$$E = \langle H \rangle \quad (21)$$

and

$$\int d\mu_a f_a = \int d\mu_b f_b = 1. \quad (22)$$

The energy, given by the statistical average of the Hamiltonian, is

$$\begin{aligned} \langle H \rangle &= \frac{1}{2} M_a \int d\mu_a f_a v_a^2 + \frac{1}{2} M_b \int d\mu_b f_b v_b^2 \\ &+ \pi G M_a^2 \int d\mu_a \int d\mu'_a |x_a - x'_a| f_a f'_a \\ &+ \pi G M_b^2 \int d\mu_b \int d\mu'_b |x_b - x'_b| f_b f'_b \\ &+ 2\pi G M_a M_b \int d\mu_a \int d\mu_b |x_b - x_a| f_a f_b, \end{aligned} \quad (23)$$

where  $\mu'_a = (x'_i, v'_i)$ ,  $f'_a = f(\mu'_a)$ , and  $M_a$  is the total mass of particles of type  $a$ , such that  $M_a = N_a m_a$ . Introducing Lagrange multipliers  $\beta, \gamma_a, \gamma_b$ , let

$$I = s + \beta(E - \langle H \rangle) + \gamma_a \left( 1 - \int d\mu_a f_a \right) + \gamma_b \left( 1 - \int d\mu_b f_b \right). \quad (24)$$

We need to find  $f_a$  and  $f_b$  such that

$$\delta_a I = \delta_b I \equiv 0, \quad (25)$$

where  $\delta_a$  represents the variation with respect to  $f_a$ , and similarly for  $\delta_b$ . Linearizing in  $\delta f_a$  and  $\delta f_b$ , we find

$$\begin{aligned} \delta_a I &= -\alpha_a \int d\mu_a \delta f_a (1 + \ln f_a) - \beta \frac{M_a}{2} \int d\mu_a \delta f_a v_a^2 \\ &- \pi G \beta M_a^2 \int d\mu_a \delta f_a \int d\mu'_a |x_a - x'_a| f'_a \\ &- \pi G \beta M_a^2 \int d\mu'_a \delta f'_a \int d\mu_a |x_a - x'_a| f_a \\ &- 2\pi G \beta M_a M_b \int d\mu_a \delta f_a \int d\mu_b |x_b - x_a| f_b \\ &- \gamma_a \int d\mu_a \delta f_a, \end{aligned} \quad (26)$$

and similarly for  $\delta_b I$ . Collecting terms and using the symmetry of the dummy variables gives

$$\begin{aligned} \delta_a I &= \int d\mu_a \delta f_a \left[ -\alpha_a (1 + \ln f_a) - \beta \frac{M_a}{2} v_a^2 \right. \\ &- 2\pi G \beta M_a^2 \int d\mu'_a |x_a - x'_a| f'_a \\ &\left. - 2\pi G \beta M_a M_b \int d\mu_b |x_b - x_a| f_b - \gamma_a \right] \end{aligned} \quad (27)$$

and finally the first variation with respect to type  $a$  is

$$\delta_a I = \int d\mu_a \delta f_a [-\alpha_a (1 + \ln f_a) - \beta M_a h(v_a, x) - \gamma_a] = 0, \quad (28)$$

where

$$h(v_a, x) = \frac{1}{2} v_a^2 + \varphi(x) \quad (29)$$

and

$$\begin{aligned} \varphi(x) &= 2\pi G \left[ M_a \int dx' |x - x'| n_a(x') \right. \\ &\left. + M_b \int dx' |x - x'| n_b(x') \right] + \text{const} \end{aligned} \quad (30)$$

is the gravitational potential. In Eq. (30)

$$n_a(x') = \int f_a(x', v) dv \quad (31)$$

is the single-particle density function for particles of mass  $a$  and similarly for mass  $b$ . The term in  $[\ ]$  in Eq. (28) must equal zero; therefore,

$$-\alpha_a (1 + \ln f_a) - \beta M_a h(v_a, x) - \gamma_a = 0. \quad (32)$$

Solving for  $f_a(v_a, x)$  gives

$$f_a(v_a, x) = e^{-(1 + \gamma_a/\alpha_a)} e^{-(\beta M_a/\alpha_a) h(v_a, x)} \quad (33)$$

and similarly for  $f_b(v_b, x)$ .

A solution for  $\varphi(x)$  is needed to substitute back into the equations for  $f_a$  and  $f_b$ . If the equation for  $\varphi(x)$  cannot be solved in an obvious manner analytically, it can be done numerically. First note that Poisson's equation for the total density is

$$\begin{aligned} \frac{d^2 \varphi(x)}{dx^2} &= 4\pi G [\rho_a(x) + \rho_b(x)] \\ &= 4\pi G [M_a n_a(x) + M_b n_b(x)]. \end{aligned} \quad (34)$$

It is clear from Eq. (33) that in order to normalize the probability density, the term multiplying the exponential must be the partition function

$$Z_a = \int d\mu_a^2 e^{-(\beta M_a/\alpha_a)[(1/2)v^2 + \varphi(x)]}. \quad (35)$$

To obtain  $n_a(x)$  and  $n_b(x)$  the  $v$  dependence in  $Z_a$  and  $Z_b$  is integrated out to get reduced partition functions for both mass types,

$$\begin{aligned} z_a &= \int dx' e^{-(\beta M_a/\alpha_a)\varphi(x')} \\ \text{and} \\ z_b &= \int dx' e^{-(\beta M_b/\alpha_b)\varphi(x')} \end{aligned} \quad (36)$$

and therefore

$$n_a(x) = \frac{1}{z_a} e^{-a\varphi(x)} \quad \text{and} \quad n_b(x) = \frac{1}{z_b} e^{-b\varphi(x)} \quad (37)$$

where

TABLE I. Constants  $A$ ,  $B$ ,  $z_a$ , and  $z_b$ .

Mass ratio ( $b/a$ )	$A$	$B$	$z_a$	$z_b$
2:1	0.1962125883	0.3037874117	2.4502466167	1.5825844396
3:1	0.1639079303	0.3360920697	2.9331663805	1.4304688333
5:1	0.1238967947	0.3761032053	3.8804008776	1.2782907030

$$a = \frac{\beta M_a}{\alpha_a} \quad \text{and} \quad b = \frac{\beta M_b}{\alpha_b}. \quad (38)$$

Differentiating with respect to  $\varphi(x)$  and rearranging gives

$$n_a = \frac{-1}{a} \frac{dn_a}{d\varphi} \quad \text{and} \quad n_b = \frac{-1}{b} \frac{dn_b}{d\varphi}. \quad (39)$$

Substituting this into Poisson's equation, Eq. (34), leads to

$$\frac{d^2\varphi}{dx^2} + 4\pi G \left[ \frac{M_a}{a} \frac{dn_a}{d\varphi} + \frac{M_b}{b} \frac{dn_b}{d\varphi} \right] = 0, \quad (40)$$

giving

$$\frac{d^2\varphi}{dx^2} + 4\pi G \frac{d}{d\varphi} \left[ \frac{M_a n_a}{a} + \frac{M_b n_b}{b} \right] = 0. \quad (41)$$

It is possible to show that

$$\frac{1}{2} \left( \frac{d\varphi}{dx} \right)^2 + 4\pi G \left[ \frac{M_a n_a}{a} + \frac{M_b n_b}{b} \right] = \text{const} \quad (42)$$

is an integral invariant of Eq. (41) thus reducing it to a first-order differential equation. Substituting Eq. (37), the exponential forms for  $n_a$  and  $n_b$ , into Eq. (42) gives

$$\frac{1}{2} \left( \frac{d\varphi}{dx} \right)^2 + A e^{-a\varphi(x)} + B e^{-b\varphi(x)} = \text{const}, \quad (43)$$

where  $A$  and  $B$  are also constants. The constants  $A$  and  $B$  can be determined by analyzing the boundary conditions. Symmetry considerations at  $x=0$  give

$$\varphi(0) = 0 \quad (44)$$

and

$$\left. \frac{d\varphi}{dx} \right|_{x=0} = 0. \quad (45)$$

With Eq. (43) this implies that  $A+B=\text{const}$ . The boundary condition at infinity,  $\varphi(|x|\rightarrow\infty)$ , implies

$$\varphi \rightarrow \infty \Rightarrow \left| \frac{d\varphi}{dx} \right| = \text{const}. \quad (46)$$

From the Hamiltonian Eq. (8) it is seen that far away from the mass distribution

$$\varphi(x) = 2\pi GM|x| + \text{const}. \quad (47)$$

This then gives

$$\frac{1}{2} \left( \frac{d\varphi}{dx} \right)^2 = A + B = \frac{1}{2} (2\pi GM)^2. \quad (48)$$

$M=2\pi G=1$  implies that  $A+B=\frac{1}{2}$ . The constant in Eq. (43) is therefore equal to  $\frac{1}{2}$ . Substituting  $A+B$  for the constant in Eq. (43) gives the following first-order differential equation for  $\varphi(x)$ :

$$\frac{d\varphi(x)}{dx} = [2A(1 - e^{-a\varphi(x)}) + 2B(1 - e^{-b\varphi(x)})]^{1/2}. \quad (49)$$

Equations (42) and (43) can be used to find an equation for  $A$  independent of  $B$  giving

$$A = \frac{4\pi GM_a}{a} \left[ \int_{-\infty}^{\infty} e^{-a\varphi(x)} dx \right]^{-1}. \quad (50)$$

Using Eq. (49) and the fact that  $dx = d\varphi(dx/d\varphi)$  in Eq. (50) gives

$$A = \frac{4\pi GM_a}{a} \left[ \int_{-\infty}^{\infty} \frac{d\varphi e^{-a\varphi}}{[2A(1 - e^{-a\varphi}) + 2B(1 - e^{-b\varphi})]^{1/2}} \right]^{-1}. \quad (51)$$

Rearranging and using Eq. (11) produces

$$\int_0^{\infty} \frac{d\varphi e^{-a\varphi}}{[A(1 - e^{-a\varphi}) + B(1 - e^{-b\varphi})]^{1/2}} = \frac{\sqrt{2}M_a}{aA}. \quad (52)$$

The simple substitution of  $u = e^{-a\varphi}$  and  $du = -ae^{-a\varphi}$  then gives

$$\int_0^1 \frac{du}{[A(1-u) + B(1-u^{b/a})]^{1/2}} = \frac{\sqrt{2}M_a}{A}. \quad (53)$$

Equation (53) contains two known quantities,  $M_a$  (the total mass of particles of type  $a$ ) and  $b/a$  (the ratio of the masses of type  $b$  to type  $a$ ). This equation was solved numerically for various mass ratios using a Romberg integration technique to obtain the value of the constant  $A$  and then using  $A+B=\frac{1}{2}$  to obtain the constant  $B$ . Once  $A$  and  $B$  were determined, the reduced partition functions, Eq. (36), were integrated in a similar form as Eq. (53). Table I shows the value of  $A$ ,  $B$ ,  $z_a$ , and  $z_b$  for the three mass ratios studied. Note that for a single-mass system  $A=B=0.25$ .

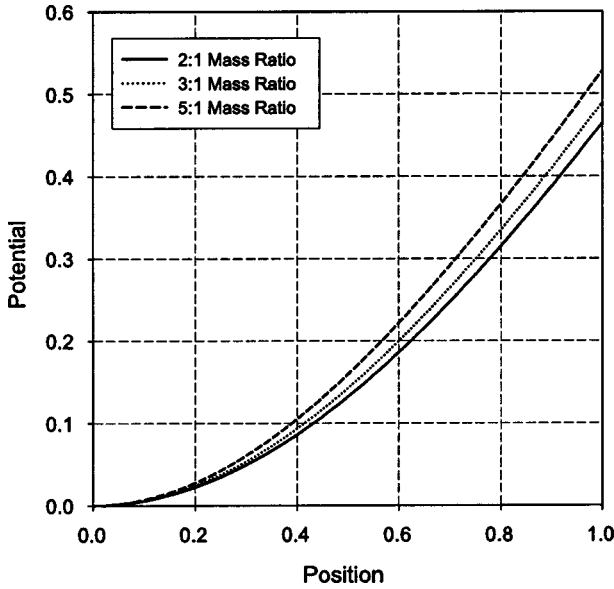


FIG. 1. Potential function from the mean-field theory for the 2:1, 3:1, and 5:1 mass ratio OGS. All units are dimensionless.

The potential function  $\varphi(x)$  is required to obtain the complete form for the density functions  $n_a(x)$  and  $n_b(x)$ . Rearranging Eq. (49) and integrating gives the following equation for  $x$  as a function of  $\varphi$ :

$$|x| = \int_0^\varphi \frac{d\varphi'}{[2A(1 - e^{-a\varphi'}) + 2B(1 - e^{-b\varphi'})]^{1/2}}. \quad (54)$$

Again, the integral can be converted to a more manageable form by making the substitution

$$u = e^{-a\varphi'} \Rightarrow e^{-b\varphi'} = u^{b/a}. \quad (55)$$

This gives the following form for the integral defining  $x$  as a function of  $\varphi$  for a particular mass ratio:

$$|x| = -\frac{1}{a} \int_1^{e^{-a\varphi}} \frac{du}{u} \{1 - 2[Au + Bu^{b/a}]\}^{-1/2}. \quad (56)$$

The integral was evaluated numerically using an adaptive step size integration technique and inverted to obtain the value of  $\varphi$  over a range of  $x$ . A cubic spline interpolation algorithm was used to obtain values for the function in the integrand for any value of  $x$  where the integral was evaluated numerically. Figure 1 shows the one-sided potential functions for all three mass ratios investigated.

The parameter  $\beta$  defines the temperature of the system. In these units, for a system with an energy of  $\frac{3}{4}$ ,  $\beta=2$ . The value of  $\beta$ , the fitted functions for  $\varphi(x)$ , the reduced partition functions  $z_a$  and  $z_b$ , and Eq. (37) provide all the elements needed to calculate the density of particles in equilibrium and compare them with the results of simulations for systems of varying mass ratio and particle number.

#### IV. TWO-MASS DYNAMICAL SIMULATIONS

The dynamical simulations of two mass-species 1D gravitational systems were run on high-speed workstations running under the Linux operating system. Since, between encounters, the particles fall freely toward each other under their mutual gravitational attraction, the solutions to simple quadratic equations are all that is required to determine the particle positions and velocities at future times. Instead of updating the entire system at each encounter, by taking advantage of the simplicity of the system clever schemes can be devised to efficiently update the positions and velocities of only the encountering particle pair and its nearest neighbors. The algorithm first calculates the time when each neighboring pair of particles will have a crossing. The smallest crossing time is found and that pair of particles is allowed to evolve up to the time of crossing. The new crossing times for that pair and their nearest neighbors is calculated, and the smallest crossing time in the list of pair crossing is found again. This process continues as the system is allowed to evolve and statistical data are taken at specific time intervals. In addition, at regular intervals the entire set of coordinates and velocities is updated to a common time and the crossing time table is recalculated as another measure in reducing cumulative numerical errors which might cause particle positions to get out of order. For systems larger than 64 particles, it is more efficient to use a binary tree to store and track the particle information rather than traditional linear storing and sorting techniques. These systems were allowed to evolve for a total time of  $10^8 \tau$ .

Two types of data files were maintained as the numerical experiments progressed. First, “snapshots” of all the particle positions and velocities were taken at fixed intervals of  $1000\tau$  for the entire length of the simulation. These snapshots are a record of the position and velocity of all system members at a particular time in the system evolution. The advantage of snapshot data is that all averages can be calculated after the completion of the simulation to save calculation time, and both forward and backward averages can be calculated if desired. In addition, calculation of particle densities and correlations is simplified with the snapshots. In the second type of data file, running averages were calculated and saved independently. These data were taken at intervals of much shorter duration than the snapshots during the early system evolution, and at longer time intervals than the snapshots during the late stages of evolution. Thus the short-time dynamics could be studied more accurately, while effective use of storage was permitted during the later stages.

For this study, the ratio of the mass of the heavy to light particles was varied as well as the total number of particles in the system. Five different system populations with three different mass ratios were investigated. The specific parameter values used are displayed in Table I. Initial conditions were generated by uniformly sampling points inside a box of fixed size in  $\mu$  space for both heavy and light particles. The size and shape of the box are determined by the total energy and the desired virial ratio, respectively. A virial ratio  $R_{virial} \approx 2$  was chosen to reduce the effects of the initial violent relaxation phase. These conditions were chosen be-



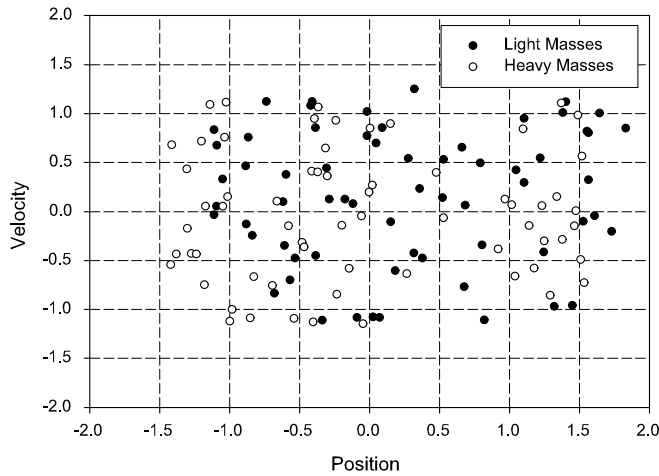


FIG. 2. Initial state ( $\mu$  space) of a 128-particle two-mass OGS with a 5:1 mass ratio. All units are dimensionless.

cause they provide an initial state that (1) is far from equilibrium, (2) has a kinetic energy ratio which is easily characterized, and (3) will rapidly approach a quasiequilibrium Vlasov state [23,26]. Since both the heavy and light particles are sampled identically inside the fixed box in  $\mu$  space, there is no equipartition of kinetic energy or mass segregation in the initial state and it is far from equilibrium. In addition, due to this sampling, the initial value of  $R_{kinetic}$  will be approximately equal to the ratio of the heavy to light masses. See Fig. 2 for a view of a typical initial state of the system in  $\mu$  space for a 5:1 mass ratio, and Fig. 3 for a view of the final state of the system in  $\mu$  space for a 5:1 mass ratio following a complete run.

## V. STATISTICAL MEASURES

In general, the ergodic properties of a system are difficult to ascertain. Ergodicity has been proven rigorously for only a handful of dynamical systems. There are, however, some indicators that are useful in determining whether a system is ergodic and mixing. The decay of correlations in time is a

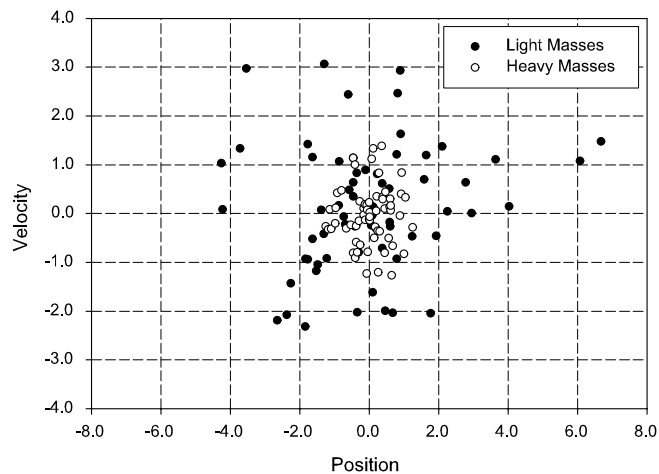


FIG. 3. Final state ( $\mu$  space) of a 128-particle two-mass OGS with a 5:1 mass ratio. All units are dimensionless.

necessary consequence of mixing behavior and is one of several measures used to analyze gravitational systems. In Paper II, equipartition of kinetic energy and mass segregation were taken as direct signs that the system was sampling the equilibrium distribution. In this study, we use dynamical simulation to test the predictions of Vlasov equilibrium theory for finite size systems. Specifically, we compare the ratio of the kinetic energies of the two mass types, the average distance from the system center of mass for the heavy and light species ( $D_H$  and  $D_L$ ), and the average particle densities of each mass type with the mean-field theory presented in Sec. III. In addition, the  $N$ -body simulations can also be used to study properties not addressed by mean-field theory. In this category we include both spatial and temporal correlation functions, and the rate of relaxation of the system towards equilibrium. We also compare the relaxation time scales of the two-species systems with those studied earlier for a single-mass component.

### A. Equipartition of kinetic energy ( $R_{kinetic}$ )

The equipartition theorem states that every coordinate that is represented by a simple quadratic expression in the Hamiltonian of a conservative system (e.g.,  $p^2/2m$ ) will, on the average, contribute  $kT/2$  to the energy.  $R_{kinetic}$ , which is the ratio of the average kinetic energy of the heavy mass particles to the light mass particles ( $R_{kinetic} = \langle KE_H \rangle / \langle KE_L \rangle$ ), is used to measure equipartition. As a thermodynamic system relaxes, the system members begin to share kinetic energy equally on the average. For a system containing two types of masses, this sharing should be easily observed. Therefore, as the system relaxes, the ratio  $R_{kinetic}$  should approach a value of unity. This is a measure of macroscopic relaxation to equilibrium. In an isolated system with a finite number of particles such as the OGS (microcanonical ensemble), however, the equipartition theorem may be exact only in the limit of large  $N$ .

### B. Mass segregation of heavy and light particles ( $D_H$ and $D_L$ )

As the system evolves in time and equipartition of kinetic energy begins, the heavy particles are transferring some of their kinetic energy to the lighter ones. While the system continues to relax, the light particles move farther out from the center of the system forming a halo, and the heavy particles move in toward the center forming a core, in a process called mass segregation. As the system evolves we can track this process by computing the time average of the distance from the origin for both the heavy ( $D_H$ ) and light ( $D_L$ ) masses. The separation of these quantities is another good indication that the system may be macroscopically relaxing to an equilibrium configuration and is closely related to  $R_{kinetic}$ .

### C. Particle density averages [ $\langle N_{m,j}(t) \rangle$ ]

Throughout the time of the simulations, data are taken on the density of particles of each mass type ( $m=H$  or  $L$  for heavy or light) in the configuration space. For each mass type, bins of equal probability were created based on the

mean-field theory discussed previously. These bins vary in size but are scaled so that each bin will contain 5% of the particles for a system in equilibrium. Since the potential is symmetric about the origin, the statistics of the corresponding bins on each side of the origin are combined during the data collection of the simulations. To create the bins, the respective density functions, Eq. (37), are integrated by stepping in position until the integral is equal to 0.05. This process is continued until all ten bins for the positive configuration space have been calculated. Since the system is symmetric, these bins are then mirrored to the negative space. During a simulation, at regular snapshots in time, the number of particles in each bin  $[N_{m,j}(t)]$  is counted and the results are averaged up to that simulation time. The value at the end of a complete simulation will give a good long-time average for the population of each bin. This can then be compared to the theoretical mean-field prediction to estimate the applicability of the mean-field theory to the actual dynamical system.

#### D. Relaxation measure $[\sigma_m^2(t)]$

To track the relaxation of the density to the equilibrium prediction, we compare the average density in each bin at the time  $t$  and  $2t$ . To quantify the difference, we define the statistical function of time,  $\sigma_m^2(t)$ , as follows:

$$\sigma_m^2(2t) = \frac{1}{N_{bin}} \sum_{j=1}^{N_{bin}} [\langle P_{m,j}(2t) \rangle - \langle P_{m,j}(t) \rangle]^2 \quad (57)$$

where

$$\langle P_{m,j}(t) \rangle = \frac{2N_{bin}}{N} \langle N_{m,j}(t) \rangle \quad (58)$$

is the time averaged population of bin  $j$  up to time  $t$  normalized to the theoretically determined number of particles per bin, and the  $m=(H,L)$  indicates either the heavy or light masses. This measure is similar to a variance if we consider the value at the later time,  $2t$ , as the true mean. Alternatively we can think of  $\sigma_m^2(t)$  as a metric between vectors  $P_{m,j}(t')$  at different times. The rate at which this measure decreases may give useful insights into how these systems relax. For example, linear decay on a log-linear plot would indicate exponential decay in time and a characteristic decay time to relaxation could be defined. On the other hand, linear decay on a log-log plot would imply a power-law decay and no characteristic decay time.

#### E. Bin correlation

Useful information concerning the spatial correlation of particle pairs can be obtained by computing the correlation of populations in different bins. The bin correlation for each mass type is calculated in the following manner: The average and the variance for each bin is first calculated using the entire dataset covering the full duration of the simulation using

$$\sigma_{n,j}^2 = \langle (N_{n,j} - \langle N_{n,j} \rangle)^2 \rangle \quad (59)$$

where  $n$  indicates the mass types, and  $j$  indicates the bin number. Next, the correlation between mass types in specific bins at a specific time  $C_{m,i;n,j}(t)$  is calculated using

$$C_{m,i;n,j}(t) = \frac{\langle [N_{m,i}(t) - \langle N_{m,i} \rangle][N_{n,j}(t) - \langle N_{n,j} \rangle] \rangle_t}{\sigma_{m,i} \sigma_{n,j}}, \quad (60)$$

where  $N_{n,j}(t)$  is the population of mass type  $n$  in bin  $j$  at time  $t$  of the simulation and the average  $\langle \rangle_t$  is taken up to time  $t$ .

#### F. Time correlation $[C(t)]$

We can learn about the duration of memory in the system by studying correlations in time. In order to investigate the possibility of the presence of long-time oscillations or normal modes that might develop as the system relaxes, correlations of the macroscopic kinetic energy ratio  $R_{kinetic}$  were computed for a steady progression of time delays. Since earlier studies of the single-component system suggested that it exists in one of several macrostates for periods of about  $10^6 \tau$ , the data were averaged over sequential blocks of  $60\,000 \tau$  dimensionless time units. The time correlation function  $C_k(t)$  essentially gives the average of the product of the fluctuations of a variable measured at time separation  $t$ . Thus the time correlation in  $x$  is defined

$$C_k(t) = \left[ \frac{1}{N-k} \sum_{j=1}^{N-k} x_j x_{j+k} \right] - \langle x \rangle^2, \quad (61)$$

where  $N$  is the total number of data points,  $j$  labels each block of duration  $t=60\,000k\tau$ , and  $x_j$  is the average of  $R_{kinetic}$  within block  $j$ .

#### G. Equipartition measure $[\Delta(t)]$

In their studies of a single-component system, Tsuchiya *et al.* [20,21] proposed a test for the equipartition of total energy  $\Delta(t)$  as a measure of phase-space ergodicity. For a system that is completely ergodic over the energy surface, the value of a macroscopic observable is simply the time average of the corresponding microscopic operator over an infinite time period. Equipartition of total energy is the equal division of energy among the members of a dynamical system over an indefinitely long time period. In the conclusions we will explain that this is a necessary, but insufficient, manifestation of ergodicity [22]. In the infinite time limit, the average of the energy per unit mass (specific energy)  $\varepsilon_i$  will achieve a unique value for all  $i$ ,

$$\varepsilon_i = \lim_{T \rightarrow \infty} \frac{1}{T} \int_0^T \varepsilon_i(t) dt = \varepsilon_0 \equiv \frac{5E}{3} \quad (62)$$

for a system with a single-mass species.

Convergence to equipartition can be quantified by introducing  $\Delta(t)$  defined by

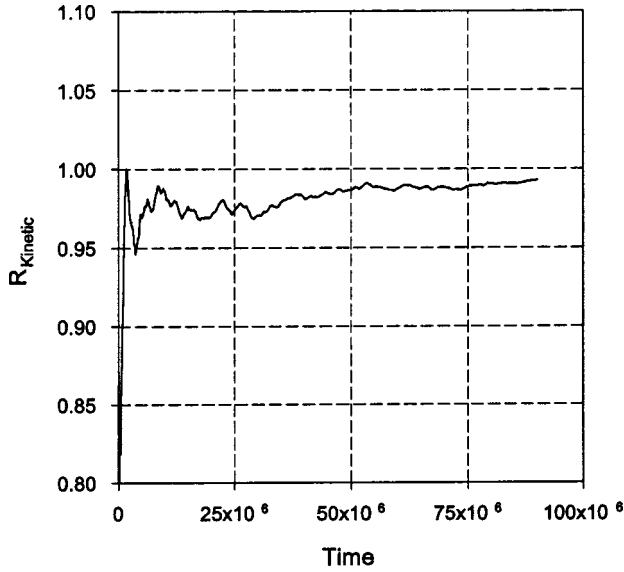


FIG. 4. Linear plot of  $R_{kinetic}$  for a 128-particle systems with a 2:1 mass ratio backward averaged over the last  $90 \times 10^6 \tau$  of the simulation. All units are dimensionless.

$$\Delta(t) \equiv \frac{1}{\varepsilon_0} \left( \frac{1}{N} \sum_{i=1}^N [\overline{\varepsilon}_i(t) - \varepsilon_0]^2 \right)^{1/2}, \quad (63)$$

where  $\overline{\varepsilon}_i(t)$  is the averaged value of the specific energy up to a time  $t$ . Therefore,  $\Delta(t)$  measures the deviation of the average energy per particle from the theoretical equipartition value. If a system is sampling the equilibrium ensemble,  $\Delta(t)$  will trend monotonically toward zero. However, the vanishing of  $\Delta(t)$  is not a guarantee of equilibrium, and can occur for other ensembles.

## VI. SIMULATION RESULTS AND COMPARISON TO THEORY

Using the algorithm discussed in Sec. IV, simulations were carried out for three different mass ratios (2:1, 3:1, and 5:1) and four different populations ( $N=16, 32, 64, 128$ ) for a duration of  $10^8$  time units. For all runs, the statistical quantities defined in the preceding section were computed. We first consider the behavior of the kinetic energy ratio of the two species,  $R_{kinetic}$ . In all cases we found that as time progressed,  $R_{kinetic}$  approached the equilibrium value of unity. Important insights can be gained by studying how this limit is approached.

Figure 4 shows a lin-log plot of  $R_{kinetic}$  for a 128-particle system with 2:1 mass ratio. This graph is a continuous average of the last  $90 \times 10^6 \tau$  in the negative time direction starting at the end of the run, i.e., a backward average. By stopping the backward average after  $90 \times 10^6 \tau$  we reduce the effect of the initial transients due to violent relaxation. In Paper II this backward average was also calculated using data averaged over windows of  $60\,000\tau$ . In that case  $R_{kinetic}$  appeared to rapidly approach the expected value of unity. Here we see  $R_{kinetic}$  approaching unity more slowly as the simulation progresses since the effect of fluctuations in time

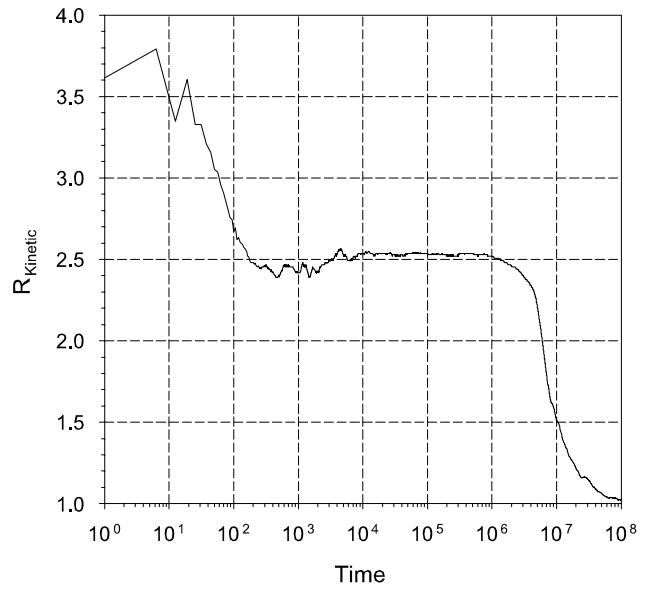


FIG. 5. Lin-log plot of  $R_{kinetic}$  for a 64-particle system with a 2:1 mass ratio forward averaged over the entire length of the simulation. All units are dimensionless.

is not reduced by local averaging. The results for all system populations and mass ratios were similar. Of course, as the system populations increase the statistical fluctuations decrease.

$R_{kinetic}$  was also averaged in the forward direction using the complete dataset from the initiation of the simulation. Figure 5 is a lin-log plot of a forward averaged  $R_{kinetic}$  for a 64-particle system with a 2:1 mass ratio. Notice that the initial value will closely, but not exactly, represent the system mass ratio. Also note the presence of a long lasting plateau from about  $2 \times 10^2 \tau$  until  $10^6 \tau$  where the curve begins to dip down toward unity. We should be mindful that this is a logarithmic plot, so early times are emphasized in the figure. In fact, the remainder of the evolution is also very gradual. The dip at  $10^6 \tau$  occurs at approximately the same time as the onset of mass segregation.

To quantify the long lasting memory effects discussed above, a time correlation function  $C_k(t)$  was also calculated for  $R_{kinetic}$  [see Eq. (61)] for a 64-particle system with a 3:1 mass ratio using the  $60\,000\tau$  windowed data. Figure 6 shows the time correlation function rapidly descending toward zero early, then slowly rising to a local maximum approximately  $10^7 \tau$  later, and finally dropping back down to near zero indicating the possible existence of long-time low frequency modes in the system.

Mass segregation, the spatial separation of different mass species, is quantified by  $D_H$  and  $D_L$  and occurred in all runs. Figures 7, 8, and 9 show lin-log plots of  $D_H$  and  $D_L$  versus time for 128-particle systems with 2:1, 3:1, and 5:1 mass ratios, respectively. Here as well we see a transient period followed by a long plateau where the segregation seems stationary (but see the comment above concerning Fig. 5). Then, after about  $10^6 \tau$ , a period of rapid divergence is again initiated, and then tapers off towards the end of the run. The mean-field predictions for the equilibrium values of  $D_H$  and

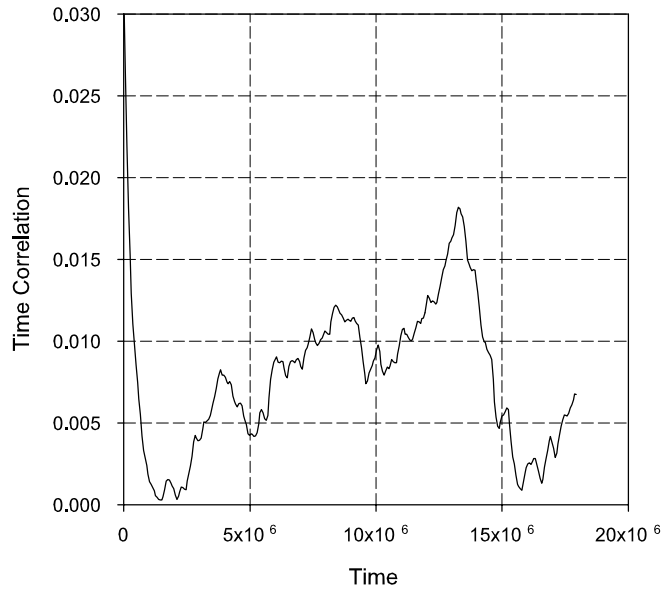


FIG. 6. Linear plot of the time correlation function of  $R_{kinetic}$  for a 64-particle system with a 3:1 mass ratio using the sliding window of width 60 000 $\tau$ . All units are dimensionless.

$D_L$  are also indicated on the graphs. Note that the times where the curves for the heavy and light masses begin to diverge are approximately equal for all three mass ratios. We see that by the end of the run the time averaged quantities have not yet achieved their equilibrium values. We also see that there is no apparent dependence of the relaxation time on the mass ratio for this process.

Comparison of time scales for mass segregation between

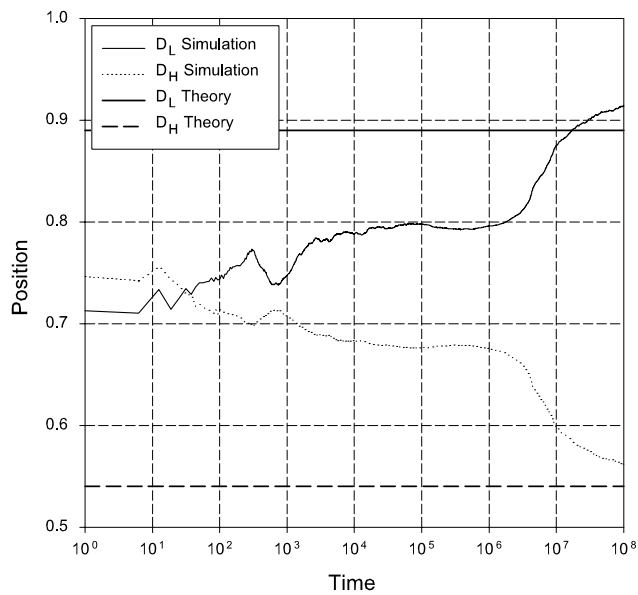


FIG. 7. Mass segregation for a 128-particle systems with a 2:1 mass ratio. The vertical axis shows ( $D_H$  and  $D_L$ ) the average of the absolute value of the distance from the origin for the light and heavy masses. Predictions from theory are indicated by the horizontal lines. All units are dimensionless.

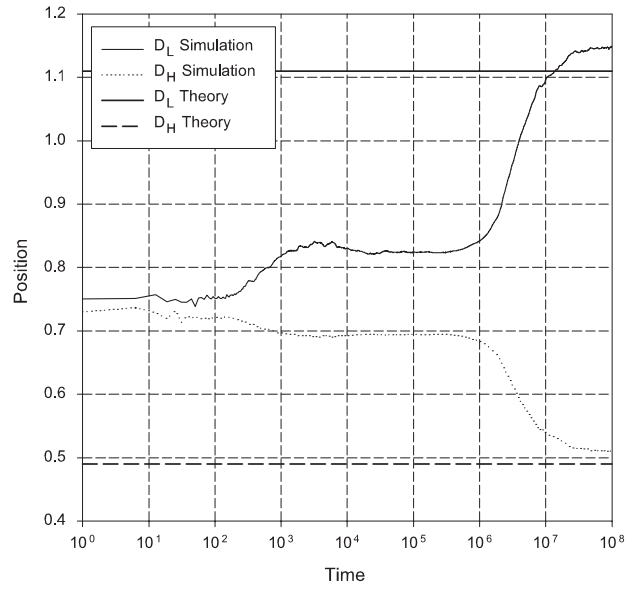


FIG. 8. Mass segregation for a 128-particle systems with a 3:1 mass ratio. The vertical axis shows ( $D_H$  and  $D_L$ ) the average of the absolute value of the distance from the origin for the light and heavy masses. Predictions from theory are indicated by the horizontal lines. All units are dimensionless.

systems of different populations did not reveal any obvious pattern either. However, the segregation time scales for the two smaller systems (16 and 32 particles) were significantly shorter than for the larger systems (64 and 128 particles) with segregation for the 32-particle 3:1 mass ratio system being the shortest clear transition. Although it may be seren-

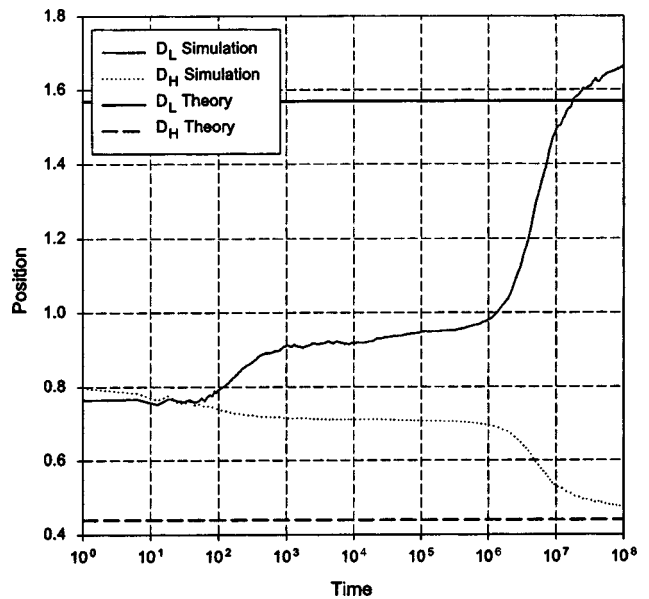


FIG. 9. Mass segregation for a 128-particle systems with a 5:1 mass ratio. The vertical axis shows ( $D_H$  and  $D_L$ ) the average of the absolute value of the distance from the origin for the light and heavy masses. Predictions from theory are indicated by the horizontal lines. All units are dimensionless.



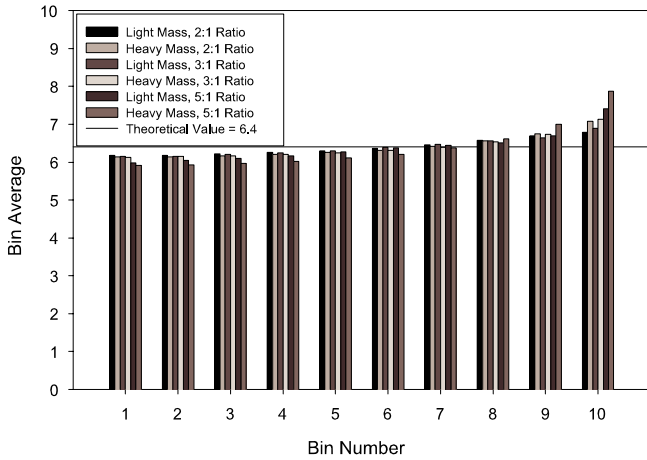


FIG. 10. Bin average data for 128-particle systems with 2:1, 3:1, and 5:1 mass ratios. The vertical axis is the average number of particles in each bin and the horizontal axis labels the bin number. Data for both the heavy and light masses are shown. The theoretically predicted value is shown as the horizontal line at the value of 6.4. All units are dimensionless.

dipitous, it is intriguing that this result matches well with those of Reidl and Miller [19] for a single-component system, where maximum mixing in phase space was seen for system sizes of approximately 30 particles.

To directly compare mean-field (Vlasov) theory with the simulations, the configuration space was partitioned into bins of equal probability according to the theory (see Sec. III). In the simulations, the time averaged population of each bin was calculated over the course of the run. The results for 128-particle systems with mass ratios of 2:1, 3:1, and 5:1 are shown in the summary chart, Fig. 10.

In Fig. 10 we label the bins according to their distance from the system center. A general trend is seen in which the bin population increases with the distance from the system center. Thus, when compared with the theoretical predictions, the inner bins are slightly underpopulated while the outer bins are overpopulated. It is important to recognize that the outer boundary of the last bin is at infinity. In general, agreement with theory is better for both the lighter mass components and the smaller mass ratios.

The relaxation measure  $\sigma_m^2(t)$  was calculated by comparing the complete dataset of bin populations at the times  $t$  and  $2t$  [Eq. (57)]. Thus, as a run progresses, the relative separation in time between the data points is ever increasing. Figure 11 shows  $\sigma_m^2(t)$  for a 128-particle system with a 2:1 mass ratio plotted on a log-log scale. Linear decay with a slope of approximately  $-1$  is observed both before and after the peak. The occurrence of this peak coincides with the transitions of both  $R_{kinetic}$  and mass segregation. The final linear decay indicates that the system is asymptotically approaching a stationary or quasiperiodic distribution while the slope indicates power-law decay and the lack of a characteristic decay time to equilibrium for the system.

The results for  $\sigma_m^2(t)$  are very similar to the equipartition measure  $\Delta(t)$  from Paper I for a system with a single-mass component. A typical log-log plot of  $\Delta(t)$  for a single-mass

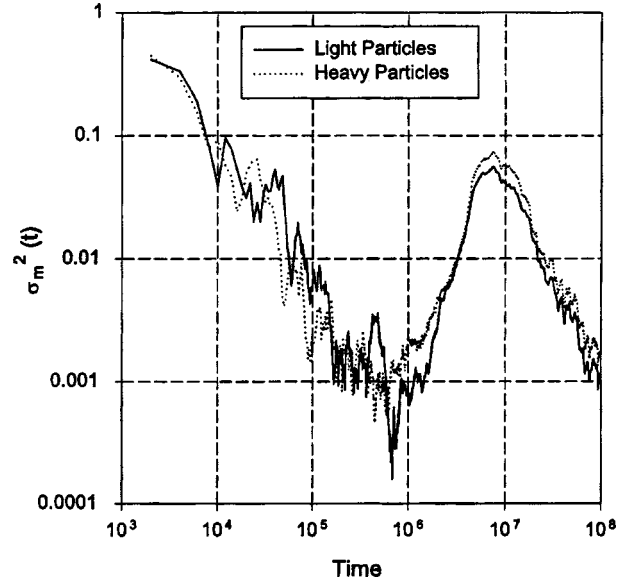


FIG. 11. Log-log plot of  $\sigma_m^2(t)$  for a 128-particle system with a 2:1 mass ratio. Note the linear decay with slope equal to  $-1$  both before and after the peak indicating the lack of a characteristic decay time. All units are dimensionless.

system of 64 particles with similar “waterbag” initial conditions is reproduced in Fig. 12. Take special note of the linear decay with slope approximately  $-0.5$  both before and after the peak. However, the time scales for the peaks are approximately an order of magnitude different.

The correlation of bin populations,  $C_{m,i;n,j}$ , is displayed in Figs. 13 and 14 in 3D plots. They show the correlations for the light and heavy particles, respectively, of a 128-particle system with 3:1 mass ratio after a simulation of

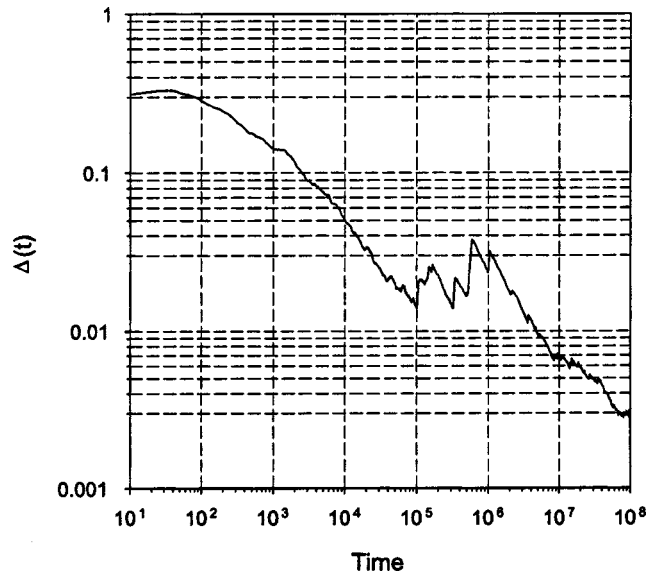


FIG. 12.  $\Delta(t)$  for a 64-particle system with the waterbag initial conditions showing an “equilibrium” peak as defined by Tsuchiya, Konishi, and Gouda followed by a general trend toward zero. All units are dimensionless.

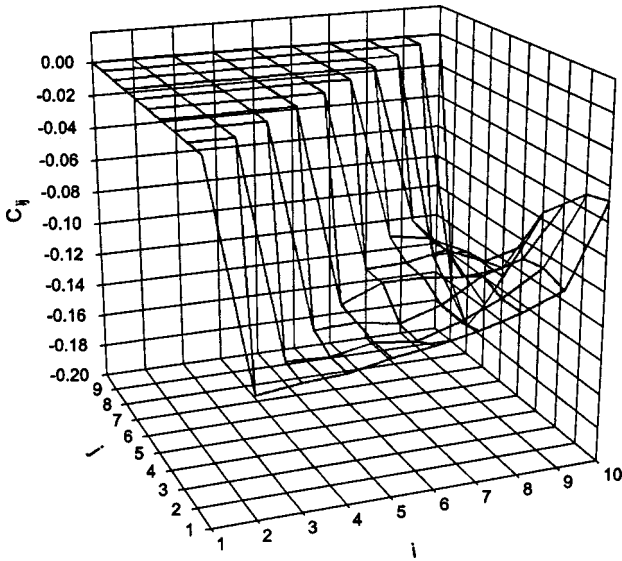


FIG. 13. Correlation of bin populations after  $10^8 \tau$  for the light masses of a 128-particle system with a 3:1 mass ratio. Note the large negative correlation between the outer bins and their nearest neighbors. All units are dimensionless.

$10^8 \tau$ . The plot for the light particles shows a large downward spike indicating a high degree of correlation between the outermost bin and its nearest neighbors. As the separation from the last bin increases, the correlation moves rapidly towards zero. For the inner bins, the correlation is somewhat flat. In the case of the heavy masses, there is a large negative correlation between the outermost bin and all other bins. The magnitude of this negative correlation increases as the separation from the outermost bin increases, i.e., moving towards the center of the system and away from the outermost bin. A

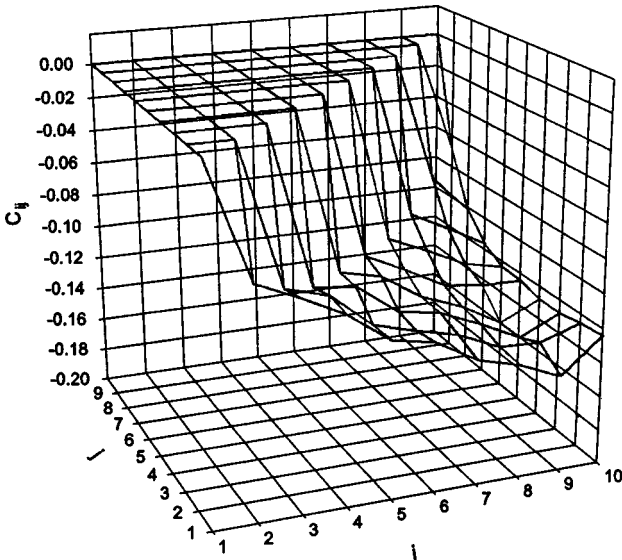


FIG. 14. Correlation of bin populations after  $10^8 \tau$  for the heavy masses of a 128-particle system with a 3:1 mass ratio. Note the large negative correlation between the innermost and outermost bins (center to edge of the system). All units are dimensionless.

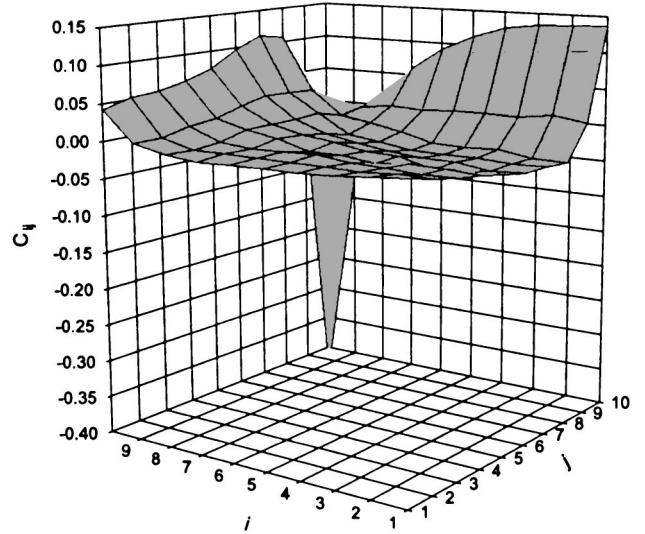


FIG. 15. Cross-correlation (light to heavy masses) of bin populations for a 64-particle system with a 3:1 mass ratio after  $10^8 \tau$ . Note the large negative correlation between the outermost bins and the increasing positive correlations between the outermost bin and the rest of the system. All units are dimensionless.

significant negative correlation occurs between the outermost and innermost bins indicating system wide influence.

The cross correlation between the heavy and light mass bin populations was also calculated for each run. Figure 15 shows the cross correlation for a 3:1 mass ratio 64-particle system. A large negative correlation is seen between the different mass types in the outermost bins, while the correlation between the outer and inner bins tends to grow more positive as the separation between bins increases. Plots of the 2:1 and 5:1 mass ratios (not shown) have similar trends with the exception that the magnitude of the correlations increases as the mass ratio becomes larger. Since the decay of correlations is closely related to relaxation, this may indicate that larger mass ratio systems have longer relaxation times. Analysis of other system sizes also showed similar trends. When comparing the cross correlations of different system sizes, the magnitude of the correlations steadily increases as the system population increases. This in turn may indicate that the relaxation time increases as a function of the system population.

VII. SUMMARY AND CONCLUSIONS

As an extension of our earlier investigation of the two-mass OGS, this paper included a larger variety of system populations and mass ratios than the study initially begun in Paper II. The original investigation was the first to definitively show mass segregation and equipartition of kinetic energy in a two-mass OGS. Here, by expanding the range of statistical tools used for the analysis the system evolution has been probed more deeply.

As a basis for the investigation, a theoretical mean-field model was developed in the Vlasov limit using the maximum entropy principle. Potential functions were derived for each

mass ratio and from these predictions for the particle densities. These predictions were compared with results from the dynamical simulations. Additional statistical measures used included spatial correlation functions and a time-dependent relaxation measure.

The following statements summarize the main results for the two-mass investigation.

(1) Dynamical simulations of all mass ratios and system sizes demonstrated that the macroscopic relaxation properties of mass segregation and equipartition of kinetic energy converge to their predicted equilibrium values.

(2) Positional correlation functions calculated from dynamical simulations showed large correlations existing even after  $10^8 \tau$  ( $\approx 10^7 t_c$ ). This represents an extremely long time in the system evolution.

(3) The  $1/t$  behavior of the relaxation measure,  $\sigma^2(t)$ , indicates the lack of a characteristic relaxation time for the system, and possible fractal structure in the phase space. In addition, it is contradictory to the exponential decay of correlations one would expect from a normal thermodynamic system exhibiting ergodic behavior. A peak in the relaxation measure occurs at the transition from the long-lived quasiequilibrium state to another state more closely representative of equilibrium.

(4) Time correlations of the ratio of kinetic energies in a system containing two-mass types showed long-time correlations on the order of  $1.4 \times 10^7 \tau$ . This is over  $2 \times 10^6$  characteristic times. In that period of time, an individual particle in a 128-particle system will have had over  $5 \times 10^8$  crossings with other system members. Clearly relaxation to equilibrium, if it occurs in this system, occurs on an extremely long time scale and weak, but significant, correlations continue to exist.

The simulations showed that mass segregation and equipartition of kinetic energy occur for all system populations and mass ratios at roughly similar times with all of them being on the order of a few million  $\tau$ . These macroscopic transitions occur at significantly later times than virialization and the rapid microscopic relaxation seen in the single-mass systems, but it is of the same order as the large first transition peaks seen later in time in  $\Delta(t)$  for the single-mass systems [20–22]. By themselves, these two simple measures are strong indicators of a transition to a final equilibrium state from a quasiequilibrium state. However, other measures such as analysis of the density and velocity distribution functions indicate that the system has not completely relaxed to the equilibrium distribution even after very long times [20,21,27]. For the limited number of runs attempted, analysis of the time scales for mass segregation and equipartition show that the macroscopic relaxation time is independent of both the system population and the mass ratio. However, the bin correlation functions indicate that the relaxation time may indeed be correlated with both the mass ratio and the system population.

An interesting feature of the relaxation measure  $\sigma_m^2(t)$  is the linear decay (on a log-log plot) that occurs both early and late in the system evolution. This  $1/t$  decay indicates that there is no characteristic time for relaxation of the system and may indicate a fractal structure to the phase space.

Klinko and Miller have shown similar results in a system of concentric spherical shells with angular momentum [35]. However, the decay for that system was strictly monotonically decreasing on average. In this case, the regions of  $1/t$  decay were separated by a large peak whose timing corresponded with other features of the system dynamics such as mass segregation, and equipartition of kinetic energy. This initial decay is representative of the long-lived quasiequilibrium state. As the system transitions from this state to one more closely representative of equilibrium, the peak in  $\sigma_m^2(t)$  begins to form as it measures differences in the two states over the  $2t-t$  time interval. This peak in  $\sigma_m^2(t)$  was very reminiscent of those that occurred in  $\Delta(t)$  for the single-mass system. Following this transition,  $\sigma_m^2(t)$  is then measuring the approach to the new state at both  $t$  and  $2t$ , and the  $1/t$  decay is again evident.

As a direct comparison with the mean-field theory, the configuration space was divided into bins of equal probability calculated from the theory. During the simulation a running average of the population of each bin was kept. At the conclusion of the simulation the average population of each bin was compared to the theoretically predicted value. It was noted that in all cases the simulations followed the predicted densities fairly well with the inner bins being slightly underpopulated and the outer bins slightly overpopulated. These results hold for the larger 128-particle systems as well. This would also be consistent with results found by Tsuchiya *et al.* in which an overabundance of higher energy particles was found to be present in the distribution for a single-mass system that otherwise looked very similar to the isothermal distribution [21]. These higher energy particles tended to reside, on average, farther out in the tail of the density distribution. This is reflected in the overshoot of  $D_L$  seen in the mass segregation plots.

Another interesting result came from the bin correlation. These results reinforced to some degree the results of the bin population averages. The correlation measure showed larger negative correlations between the outermost bin and all other bins. In addition, the plots of the bin correlation for the light and heavy masses were quite dissimilar with the light masses showing an unusual negative correlation spike between the outermost bin and its nearest neighbor. This spike was not seen in the heavy mass correlations where there was a roughly consistent negative correlation between the outermost bin and all other bins.

The bin cross correlation of the different mass types indicated a correlation between relaxation time and both mass ratio and system population. The magnitude of the cross correlations increased as the mass ratio and the system population increased. This implies that the relaxation time (related to the time scale of the decay of correlations in the system) increases as the mass ratio and the system population increase. A large negative correlation between the light and heavy masses in the outermost bins was evident in all systems as well as large positive correlations between the outermost bin and all other bins.

Substantial work has been done on the OGS over more than 30 years; however, the question of ergodicity and relaxation is still an open issue. This paper has shown that two-



mass systems exhibit several features normally associated with systems either approaching or that have already attained equilibrium, however, substantial correlations still exist after simulation times exceeding  $10^8 \tau$ . This suggests that collective motion may take place over very long times. This type of behavior has been previously observed in Vlasov simulations of the OGS [12]. In addition, some of the differences noted between the Vlasov theory and simulation results (e.g., in the bin population studies) must be due to finite size effects, although this was not indicated in other measures for the range of system populations studied here (e.g., the time scale for mass segregation). Finite size effects may be masked by differences in the initial conditions.

In these numerical experiments consideration of the evolution of both average quantities and correlations suggest the following scenario: The system rapidly relaxes to a quasistationary state. We conjecture that this state is “close” to a stationary Vlasov state, of which there are many (since for the latter  $N \rightarrow \infty$  they cannot be identical). At present we lack the ability to predict this state from the set of initial conditions. The system then appears to slowly, but continuously, evolve through a sequence of quasistationary states until it finally approaches thermal equilibrium. As in higher-dimensional systems we expect that, as  $N$  increases, the time to approach equilibrium will also increase and thus become more difficult to observe in simulations. Thus we could say that in gravitational systems relaxation itself is a discreteness effect. It is especially hard to observe in one-dimensional systems because, at crossings, only the acceleration of the crossing pair changes so the mixing is very slow. Thus we have shown here that there is a window in population where we can observe that the system approaches the equilibrium state. For smaller values of  $N$ , as was demonstrated for the

single-mass system, the phase space may be segmented into stable and unstable regions in which it will be trapped [17,18]. For larger values of  $N$  we expect equilibration on longer times, but to see it will require an extensive computational effort. We anticipate that for sufficiently large  $N$  there is a scaling region where the  $N$  dependence of the evolution is more pronounced. However, we have not seen evidence for this for the system sizes we were able to simulate. It would be interesting if in fact the scaling behavior could be determined from theory.

Clearly, based upon these results as well as those of other researchers, it is still not possible to draw a definitive conclusion on the question of relaxation in the OGS. However, the general results of these studies suggest that equilibrium is being approached. The evolution of global measurements of the macroscopic behavior of the one-dimensional self-gravitating system indicates that the system is relaxing to the equilibrium state in a finite, but very long time, while measurements of more local properties of the system, such as time averaged probability densities, are within a few percent of the equilibrium values, but have not completely converged. What is clear, however, is that these systems exhibit very weak diffusion, extremely long correlations in time, and weak ergodic properties in the phase space. Future work may need to include more thorough studies of other correlations in the system as well as an investigation of the possible fractal structure in the phase space.

#### ACKNOWLEDGMENTS

The authors are grateful for the support of the Research Foundation and the Division of Information Services of Texas Christian University.

- 
- [1] E. Fermi, J. R. Pasta, and S. Ulam, *Collected Works of Enrico Fermi* (University of Chicago Press, Chicago, 1965), Vol. 2, p. 978.
  - [2] J. Binney and S. Tremaine, *Galactic Dynamics* (Princeton University Press, Princeton, NJ, 1987).
  - [3] J.H. Oort, *Bull. Astron. Inst. Neth.* **6**, 289 (1932).
  - [4] G.L. Camm, *Mon. Not. R. Astron. Soc.* **110**, 305 (1950).
  - [5] D. Lynden-Bell, *Mon. Not. R. Astron. Soc.* **136**, 101 (1967).
  - [6] L. Cohen and M. Lecar, *Bull. Astron.* **3**, 213 (1968).
  - [7] S. Cuperman, A. Hartman, and M. Lecar, *Astrophys. Space Sci.* **13**, 397 (1971).
  - [8] G. Rybicki, *Astrophys. Space Sci.* **14**, 56 (1971).
  - [9] J.J. Monaghan, *Aust. J. Phys.* **31**, 95 (1978).
  - [10] Y. Fukui and T. Morita, *Aust. J. Phys.* **32**, 289 (1979).
  - [11] L. Reichl, *A Modern Course in Statistical Physics* (Wiley-Interscience, New York, 1998).
  - [12] P. Mineau, M.R. Feix, and J.L. Rouet, *Astron. Astrophys.* **228**, 344 (1990).
  - [13] G. Benettin, C. Froeschle, and J.P. Scheidecker, *Phys. Rev. A* **19**, 2454 (1979).
  - [14] H.L. Wright, B.N. Miller, and W.E. Stein, *Astrophys. Space Sci.* **84**, 421 (1982).
  - [15] M. Luwel, G. Severne, and J. Rousseeuw, *Astrophys. Space Sci.* **100**, 261 (1984).
  - [16] C.J. Reidl and B.N. Miller, *Astrophys. J.* **318**, 248 (1987).
  - [17] C.J. Reidl and B.N. Miller, *Phys. Rev. A* **46**, 837 (1992).
  - [18] C.J. Reidl and B.N. Miller, *Phys. Rev. E* **48**, 4250 (1993).
  - [19] C.J. Reidl and B.N. Miller, *Phys. Rev. E* **51**, 884 (1995).
  - [20] T. Tsuchiya, T. Konishi, and N. Gouda, *Phys. Rev. E* **50**, 2607 (1994).
  - [21] T. Tsuchiya, N. Gouda, and T. Konishi, *Phys. Rev. E* **53**, 2210 (1996).
  - [22] K.R. Yawn and B.N. Miller, *Phys. Rev. E* **56**, 2429 (1997).
  - [23] T. Tsuchiya, N. Gouda, and T. Konishi, *Astrophys. Space Sci.* **257**, 319 (1998).
  - [24] G. Severne, M. Luwel, and J. Rousseeuw, *Astron. Astrophys.* **139**, 365 (1984).
  - [25] F. Hohl and J. Campbell, *Astron. J.* **73**, 611 (1968).
  - [26] K.R. Yawn and B.N. Miller, *Phys. Rev. Lett.* **79**, 3561 (1997).
  - [27] L. Milanovic, H.A. Posch, and W. Thirring, *Phys. Rev. E* **57**, 2763 (1998).
  - [28] T. Tsuchiya and N. Gouda, *Phys. Rev. E* **61**, 948 (2000).
  - [29] D. Fanelli, M. Merafina, and S. Ruffo, *Phys. Rev. E* **63**, 066614 (2001).



- [30] D. Fanelli and E. Aurell, *Astron. Astrophys.* **395**, 399 (2002).
- [31] B.N. Miller and J.L. Rouet, *Phys. Rev. E* **65**, 056121 (2002).
- [32] S.F. Shandarin, A.L. Melott, K. McDavitt, J.L. Pauls, and J. Tinker, *Phys. Rev. Lett.* **75**, 7 (1995).
- [33] S.F. Shandarin and Y.B. Zeldovich, *Rev. Mod. Phys.* **61**, 185 (1989).
- [34] T. Tatakawa and K. Maeda, *Astrophys. J.* **547**, 531 (2001).
- [35] P. Klinko and B.N. Miller, *Phys. Rev. E* **65**, 056127 (2002).